Available online at www.sciencedirect.com
SCIENCE DIRECT®
Pergamon
Materials Research Bulletin 38 (2003) 11–16
Materials Research Bulletin
www.elsevier.com/locate/matresbu

Preparation of $La_{1-x}Sr_xMnO_3$ nanoparticles by sonication-assisted coprecipitation

Guangsheng Pang[a,1], Xiaonong Xu[b], Vladimir Markovich[c], Sigalit Avivi[a], Oleg Palchik[a], Yuri Koltypin[a], Gad Gorodetsky[c], Yosef Yeshurun[b], Hans Peter Buchkremer[d], Aharon Gedanken[a,*]

[a]*Department of Chemistry, Bar-Ilan University, Ramat-Gan 52900, Israel*
[b]*Department of Physics, Bar-Ilan University, Ramat-Gan 52900, Israel*
[c]*Department of Physics, Ben-Gurion University of the Negev, P.O. Box 653, Beer-Sheva 84105, Israel*
[d]*Research Centre, IWV-1 Institute for Materials and Processing in Energy Systems, Jülich D-52425, Germany*

Received 26 April 2002; received in revised form 4 June 2002; accepted 18 October 2002

Abstract

$La_{1-x}Sr_xMnO_3$ ($x = 0.3$) (LSM) nanoparticles were prepared by a sonication-assisted coprecipitation method. The coprecipitation reaction is carried out with ultrasound radiation. Lower sintering temperatures are required for the sonication-assisted product. Fully crystallized LSM with an average particle size 24 nm is obtained after the as-prepared mixture is annealed at 900 °C for 2 h. Magnetic properties indicate that the transition temperature from the paramagnetic to ferromagnetic state of the sample is quite sharp and occurs at 366 K for samples annealed for 2 h at 900 and 1100 °C.

Keywords: Nanostructures; Oxides; Magnetic properties

1. Introduction

$La_{1-x}A_xMnO_3$ (A = Ca, Sr, Ba, Pb) are important materials because of their giant magnetoresistance (GMR) properties [1]. GMR was first observed in thin films of these perovskite oxides [2–4], but it has also been observed in polycrystalline [5,6] and single-crystal samples [7]. These materials are important because of their potential applications as magnetic sensors and reading heads for magnetic memories. $La_{1-x}Sr_xMnO_3$ (LSM) is also used as a cathode in solid oxide fuel cells (SOFCs) because of

* Corresponding author. Tel.: +972-3-5318315; fax: +972-3-5351250.
E-mail addresses: panggs@mail.jl.cn (G. Pang), gedanken@mail.biu.ac.il (A. Gedanken).
[1] Present address: Department of Chemistry, Jilin University, Changchun 130023, PR China.

0025-5408/02/$ – see front matter
PII: S0025-5408(02)01002-4

its good chemical stability and thermal expansion compatibility with the solid electrolyte [8–10]. Most of the expected applications of these materials require either thin films (magnetic recording heads) or thick films (oxygen membranes in SOFCs). Until now, a large variety of methods, such as coprecipitation [11–14], sol–gel [15,16], hydrothermal [17], pulse laser deposition [18], magnetron sputtering [19], molecular beam epitaxy [20], metal organic decomposition [21], electrochemical deposition [22] and aerosol pyrolysis [23] have been used to prepare both powder and film of perovskite oxomanganates. Although there are several successful methods for the preparation of LSM films, a polycrystalline material is advantageous because it is less restricted in its substrate selection and processing parameters for deposition. In most applications, high purity and homogeneous nano-sized powders are required.

Sonochemistry has been successfully used to prepare nanoparticles. The chemical effects of ultrasound arise from acoustic cavitation, that is, the formation, growth, and implosive collapse of bubbles in a liquid [24]. In brief, during the process, the implosive collapse of the bubble generates localized hot spots through adiabatic compression or shock wave formation within the gas phase of the collapsing bubble. The extreme conditions attained during bubble collapse have been exploited to prepare amorphous metals, carbides, oxides, sulfides and composite nanoparticles [25]. There are two regions of sonochemical reactivity, the inside of the collapsing bubble and the interface between the bubble and the liquid [26]. For volatile precursors, the sonochemical reaction takes place inside the collapsing bubbles, as in the decomposition of transition-metal carbonyls, which results in an amorphous product. There are also a few reports on the synthesis of crystalline nanoparticles under sonication [27], in which the reaction occurs in the thin layer immediately surrounding the collapsing cavity.

In our efforts to synthesize nanoparticles of LSM in this project, we have combined sonochemistry with the coprecipitation method. The drawbacks of possible inhomogeneities in the coprecipitation method are avoided by forming a homogeneous colloidal suspension in ethanol. Fully crystallized LSM nanoparticles are obtained after the as-prepared nano LSM mixture is annealed at 700 °C for 2 h.

2. Experimental section

The reactants used in the synthesis are: $La(NO_3)_3{\cdot}xH_2O$ (La, 32.0%), $Sr(NO_3)_2$, $MnCl_2{\cdot}4H_2O$, $KMnO_4$ (Aldrich) and KOH (Bio Lab). A typical synthesis procedure is as follows: 3.04 g $La(NO_3)_3{\cdot}xH_2O$, 0.64 g $Sr(NO_3)_2$ and 1.46 g $MnCl_2{\cdot}4H_2O$ are mixed and dissolved in 300 ml water (Solution A) outside the sonication cell. One hundred milliliters of Solution B, which contains 0.41 g $KMnO_4$ and 11.22 g KOH, is then slowly dropped into Solution A with sonication. The molar ratios of the initial reaction mixture are $0.70La(NO_3)_3{\cdot}xH_2O$:$0.30Sr(NO_3)_2$:$0.74MnCl_2{\cdot}4H_2O$:$0.26KMnO_4$:20.00KOH. The solution is sonicated at room temperature for 30 min. The sonication is performed using a direct immersion titanium sonicator (Vibracell, 20 kHz, 100 W/cm^2). The titanium horn is dipped (1 cm) in the solution, and the solution is thoroughly mixed. A complete precipitation is obtained only after 30 min. If the reaction is stopped earlier, a smaller amount of Sr is precipitated. Longer irradiation times did not increase the amount of products. All the reactions are performed under normal air conditions. During sonication, the temperature of the reaction mixture rises to ca. 80 °C. The suspension is centrifuged and then washed with distilled water five times. The product is suspended in ethanol under sonication for 10 min, and then the ethanol is evaporated by heating at 110 °C to obtain the dry product. Fully

crystallized LSM nanoparticles are obtained after the as-prepared sample is annealed in air at 700 °C for 2 h.

Powder X-ray diffraction (XRD) analysis is performed on a Rigaku 2028 diffractometer with nickel-filtered Cu Kα radiation. Particle size is calculated from the X-ray line broadening, using the Debye–Scherrer equation. The transmission electron micrographs (TEM) are obtained by using a JEOL-JEM 100SX microscope. Samples for TEM are prepared by placing a drop of the sample suspension on a copper grid (400 mesh, Electron Microscopy Sciences) coated with carbon film, and are then allowed to dry in air. The oxidation state of manganese in the sample is determined by iodometric titration. The magnetic properties of the sample are measured with an Oxford-3001 vibrating sample magnetometer (VSM) from 130 to −193 °C, with a cooling rate of 3 °C/min. Measurements of electrical resistance and magnetoresistance (MR) are carried out on the annealed (900 °C, 2 h) powder samples. In order to enable an appropriate electrical wiring, the powder is compacted under a pressure of 0.5 GPa in a well-defined form and annealed at 1400 °C for 24 h in air. The average particle size estimated from the XRD line broadening is ca. 50 nm for the sample annealed at 1400 °C. Measurements of magnetoresistance were carried out using the customary four-point method at magnetic fields H up to 1.5 T, aligned perpendicular to the current direction.

3. Results and discussion

Fig. 1a–d shows the XRD patterns of LSM prepared at different annealing temperatures. Incipient crystallization of the LSM phase occurs after annealing at 600 °C (Fig. 1a). The XRD pattern of the sample annealed at 700 °C indicates that the sample is fully crystallized, and no impurity can be detected by XRD (Fig. 1b). The particle size is calculated from the XRD line broadening. The average particle sizes of the samples annealed at 600, 700, 900 and 1100 °C are 16, 19, 24 and 35 nm, respectively.

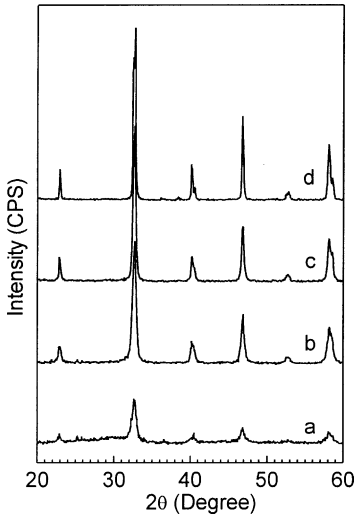

Fig. 1. XRD patterns of LSM annealing at different temperatures: (a) 600 °C, (b) 700 °C, (c) 900 °C and (d) 1100 °C.

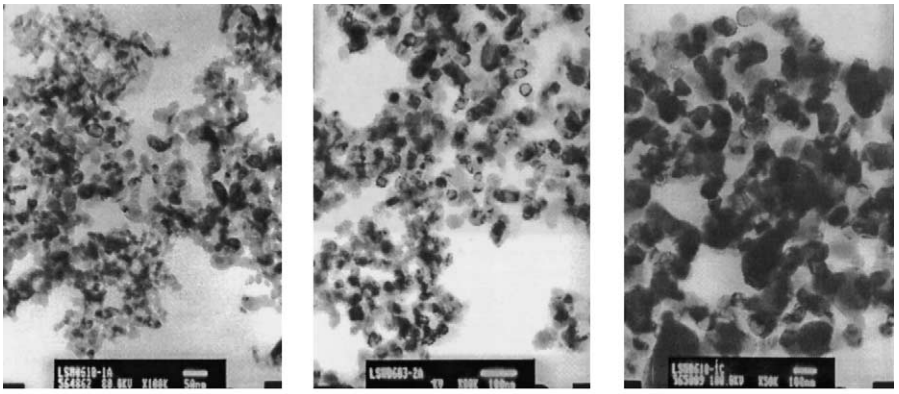

(a) (b) (c)

Fig. 2. TEM micrographs of LSM samples annealed at different temperatures: (a) 700 °C, (b) 900 °C and (c) 1100 °C.

Fig. 2a–c shows the TEM of LSM samples annealed at 700, 900 and 1100 °C, respectively. The particle size estimated from the TEM result is consistent with the XRD result. Annealing temperature plays an important role in determining the particle size. The particle size increases as the annealing temperature increases, which is also the case for the sol–gel method [5,28,29].

The oxidation state of manganese in the sample is determined by iodometric titration. The Mn^{4+} content of the samples annealed at 700, 900 and 1100 °C are 41, 35 and 35%, respectively. For the samples annealed at 900 and 1100 °C, the difference between the high valency 3.35 versus the expected valency 3.30 is less than 2%, and any theory or explanation that would be given would be speculative. A slightly higher Mn^{4+} content in the sample annealed at 700 °C is due to the fact that a small portion of $SrCO_3$ has still not decomposed at this temperature. According to the TGA results, there is a weight loss of ca. 1.0 wt.% from 700 to 900 °C, and there is no weight loss above 900 °C. It is worth noting that there is no change in the Mn^{4+} content when the samples are annealed at different temperatures, from 900 to 1100 °C. A constant Mn^{4+} content implies that the as-prepared samples have reacted completely at 900 °C. Although the annealing temperature changed from 900 to 1100 °C, the Mn^{4+} content is still stable, which is attributed to the likelihood that Mn^{3+} and Mn^{4+} in the structure of the LSM nanoparticles are homogenously distributed in the structure lattice. The EMR studies also show that the LSM nanoparticles obtained by sonication-assisted coprecipitation method are more homogeneous than the bulk crystals, which is published elsewhere [30].

Fig. 3 shows the temperature dependence of the magnetization for the LSM sample annealed at different temperatures. Both samples have a quite sharp transition temperature from a paramagnetic to a ferromagnetic state at 93 °C. This transition temperature is consistent with the reported value, 85 °C, of the transition temperature observed for a single crystal of LSM [7]. The results observed for the magnetoresistance at room temperature, are shown in Fig. 4. The MR exhibits a sharp drop in low fields followed by a lesser negative magnetoresistance at higher fields. Such a low field effect, which was observed in polycrystalline manganite ceramics, is attributed to spin-dependent grain-boundary scattering [31–33]. The high-field behavior is an intrinsic property. It appears that the behavior of the MR for $La_{1-x}Sr_xMnO_3$ ($x = 0.3$) nanoparticles prepared by a sonication-assisted coprecipitation method is similar to that obtained for ceramics LSM. The low field drop of the MR increases with decreasing of temperature similar to ceramics samples.

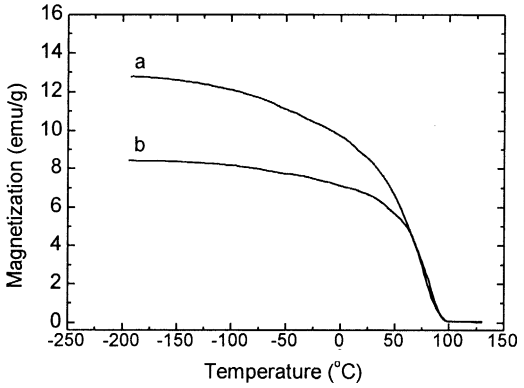

Fig. 3. Temperature dependence of the magnetization measured at magnetic field 20 G for LSM samples annealed at (a) 900 °C and (b) 1100 °C.

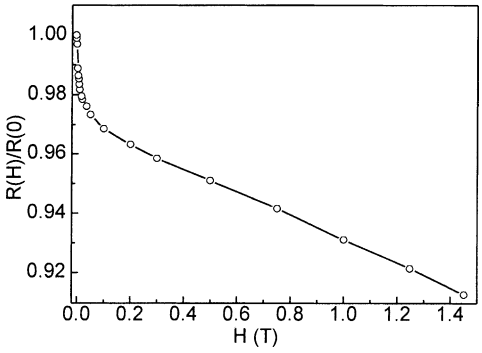

Fig. 4. Variation of magnetoresistence of LSM sample (1400 °C for 24 h) with magnetic field at room temperature.

4. Conclusion

In summary, fully crystallized LSM nanoparticles are prepared by a sonication-assisted coprecipitation method. This paper demonstrates that the advantages obtained by involving ultrasound radiation in the coprecipitation reaction are the lowering of the sintering temperature and a more homogenous distribution of Mn^{3+} and Mn^{4+} in the structure of LSM nanoparticles. Using sonication, a simple mixture is precipitated from the reaction solution. Then a stable colloidal suspension is formed by sonication, and this ensures a high degree of homogenization of the small particles of the mixture. Homogenization ensures that a lower annealing temperature is sufficient for the reaction to occur. The sonication-assisted coprecipitation is easy to extend to other complex oxide systems.

Acknowledgements

Y. Yeshurun, G. Gorodetsky, and A. Gedanken thank the Ministry of Science, Culture, and Sport for supporting this research through the Infrastructure-Strategic Project. A. Gedanken thanks also the

BMBF, Germany, for financial support through the Energy Program. Dr. Pang and Dr. Xu thank the Kort 100 Scholarship Foundation for supporting their postdoctoral fellowship. The authors also thank Dr. Shifra Hochberg for editorial assistance.

References

[1] A.P. Ramirez, J. Phys.-Condens. Mater. 9 (1997) 8171.
[2] R.M. Kusters, J. Singleton, D.A. Keen, R. McGreevy, W. Hayes, Physica B 155 (1989) 362.
[3] R. von Helmolt, J. Wecker, B. Holzapfel, L. Schultz, K. Samwer, Phys. Rev. Lett. 71 (1993) 2331.
[4] K. Chahara, T. Ohno, M. Kasai, Y. Kozono, Appl. Phys. Lett. 63 (1993) 1990.
[5] R.D. Sanchez, J. Rivas, C. Vazquez-Vazquez, A. Lopez-Quintela, M.T. Causa, M. Tovar, S. Oseroff, Appl. Phys. Lett. 68 (1996) 134.
[6] S. Jin, H.M. O'Bryan, T.H. Tiefel, M. McCormack, W.W. Rhodes, Appl. Phys. Lett. 66 (1995) 382.
[7] A. Urushibara, Y. Moritomo, T. Arima, A. Asamitsu, G. Kido, Y. Tokura, Phys. Rev. B 51 (1995) 14103.
[8] N.Q. Minh, J. Am. Ceram. Soc. 76 (1993) 563.
[9] J.H. Choi, J.H. Jang, J.H. Ryu, S.M. Oh, J. Power Sources 87 (2000) 92.
[10] T. Fukui, S. Ohara, M. Naito, K. Nogi, J. Nanopart Res. 3 (2001) 171.
[11] S.A. Prokudian, Ya.S. Rubinchik, and M.M. Pavlyuchenko, Inorg. Mater. (1974) 416.
[12] M. Uehara, K. Takahashi, T. Asaka, S. Tsutsumi, J. Ceram. Soc. Jpn. 106 (1998) 1248.
[13] M. Uehara, T. Nagai, A. Yamazaki, K. Takahashi, S. Tsutsumi, Chem. Lett. 6 (1999) 463.
[14] M. Mori, N.M. Sammes, G.A. Tompsett, J. Power Sources 86 (2000) 395.
[15] S.Y. Bae, S.X. Wang, Appl. Phys. Lett. 69 (1996) 121.
[16] C. Vazquez-Vazquez, M.C. Blanco, M. Lopez-Quintela, R.D. Sanchez, J. Rivas, S.B. Oseroff, J. Mater. Chem. 8 (1998) 991.
[17] D. Wang, R.B. Yu, S.H. Feng, W.J. Zheng, G.S. Pang, H. Zhao, Chem. J. Chin. Univ. 19 (1998) 165.
[18] T.R. McGuire, A. Gupta, R.P. Duncombe, M. Rupp, J.Z. Sun, R.B. Laibowitz, W.J. Gallager, X. Gang, J. Appl. Phys. 79 (1996) 4549.
[19] E.S. Vlakhov, R.A. Chakalov, R.I. Chakalova, K.A. Nenkov, K. Dorr, A. Handstein, K.H. Muller, J. Appl. Phys. 83 (1998) 2152.
[20] J. O'Donnell, M. Onellion, M.S. Rzchowski, J.N. Eckstein, I. Bozovic, Phys. Rev. B 54 (1996) 6841.
[21] B. Chen, C. Uher, D.T. Morelli, J.V. Mantese, A.M. Mance, A.L. Micheli, Phys. Rev. 53 (1996) 5094.
[22] G.H. Therese, P.V. Kamath, Chem. Mater. 10 (1998) 3364.
[23] E. Herrero, M.V. Cabanas, J. Alonso, F. Conde, J.M. Gonzalez-Calbet, M. Vallet-Regi, Chem. Mater. 11 (1999) 3521.
[24] K.S. Suslick (Ed.), Ultrasound: Its Chemical, Physical and Biological Effects, VCH, Weinheim, 1988.
[25] K.S. Suslick, G.J. Price, Ann. Rev. Mater. Sci. 29 (1999) 295, and references cited therein.
[26] K.S. Suslick, R.E. Cline Jr, D.A. Hammerton, J. Am. Chem. Soc. 108 (1986) 5641.
[27] S. Avivi, Y. Mastai, G. Hodes, A. Gedanken, J. Am. Chem. Soc. 121 (1999) 4196.
[28] S. Yang, C.T. Lin, K. Rogacki, B. Dabrowski, P.M. Adams, D.M. Speckman, Chem. Mater. 10 (1998) 1374.
[29] L.E. Hueso, F. Rivadulla, R.D. Sanchez, D. Caeiro, C. Jardon, C. Vazquez-Vazquez, J. Rivas, M.A. Lopez-Quintela, J. Magn. Magn. Mater. 189 (1998) 321.
[30] A.I. Shames, E. Rozenberg, G. Gorodetsky, A.A. Arsenov, D.A. Shulyatev, Ya.M. Mukovskii, A. Gedanken, G. Pang, J. Appl. Phys. 91 (2002) 7929.
[31] H.Y. Hwang, S.-W. Cheong, N.P. Ong, B. Battlogg, Phys. Rev. Lett. 77 (1996) 2041.
[32] J.M.D. Coey, M. Viret, S. von Molnar, Adv. Phys. 48 (1999) 167.
[33] A. Gupta, Low-field magnetoresistance induced by grain boundaries in doped manganese perovskites, in: C.N.R. Rao, B. Raveau (Eds.), Colossal Magnetoresistance, Charge Ordering and Related Properties of Manganese Oxides, World Scientific, Singapore, 1998.